

1 **Variants in the degron of *AFF3* cause a multi-system disorder with mesomelic dysplasia,**  
2 **horseshoe kidney and developmental and epileptic encephalopathy**

3  
4  
5 **Authors:**

6 Norine Voisin<sup>1</sup>, Rhonda E. Schnur<sup>2,3</sup>, Sofia Douzgou<sup>4,5</sup>, Susan M. Hiatt<sup>6</sup>, Cecilie F. Rustad<sup>7</sup>,  
7 Natasha J. Brown<sup>8,9,10</sup>, Dawn L. Earl<sup>11</sup>, Boris Keren<sup>12</sup>, Olga Levchenko<sup>13</sup>, Sinje Geuer<sup>14,15</sup>,  
8 David Amor<sup>9,10</sup>, Alfredo Brusco<sup>16,17</sup>, E. Martina Bebin<sup>18</sup>, Gerarda Cappuccio<sup>19</sup>, Joel  
9 Charrow<sup>20</sup>, Nicolas Chatron<sup>1,21</sup>, Gregory M. Cooper<sup>6</sup>, Elena Dadali<sup>13</sup>, Julien Delafontaine<sup>22</sup>,  
10 Ennio Del Giudice<sup>19</sup>, Ganka Douglas<sup>2</sup>, Tara Funari<sup>2</sup>, Giuliana Giannuzzi<sup>1</sup>, Nicolas Guex<sup>1,22</sup>,  
11 Delphine Heron<sup>12</sup>, Øystein L. Holla<sup>23</sup>, Anna C.E. Hurst<sup>24</sup>, Jane Juusola<sup>2</sup>, David Kronn<sup>25</sup>,  
12 Alexander Lavrov<sup>13</sup>, Crystle Lee<sup>8</sup>, Else Merckoll<sup>26</sup>, Anna Mikhaleva<sup>1</sup>, Jennifer Norman<sup>27</sup>,  
13 Sylvain Pradervand<sup>1,22</sup>, Victoria Sanders<sup>20</sup>, Fabio Sirchia<sup>28</sup>, Toshiki Takenouchi<sup>29</sup>, Akemi J.  
14 Tanaka<sup>30,31</sup>, Heidi Taska-Tench<sup>20</sup>, Elin Tønne<sup>7</sup>, Kristian Tveten<sup>23</sup>, Giuseppina Vitiello<sup>19</sup>,  
15 Tomoko Uehara<sup>29</sup>, Caroline Nava<sup>12</sup>, Binnaz Yalcin<sup>1,32</sup>, Kenjiro Kosaki<sup>29</sup>, Dian Donnai<sup>4,5</sup>,  
16 Stefan Mundlos<sup>14,15</sup>, Nicola Brunetti-Pierri<sup>19,33</sup>, Wendy K. Chung<sup>30,31</sup>, Alexandre Reymond<sup>1</sup>

17  
18 <sup>1</sup>Center for Integrative Genomics, University of Lausanne, Lausanne, CH-1015, Switzerland

19 <sup>2</sup>GeneDx, Gaithersburg, MD 20877, USA

20 <sup>3</sup>Cooper Medical School of Rowan University, Division of Genetics, Camden, NJ, 08103  
21 USA

22 <sup>4</sup>Manchester Centre for Genomic Medicine, St Mary's Hospital, Manchester University  
23 Hospitals NHS Foundation Trust, Manchester Academic Health Sciences Centre, Manchester  
24 M13 9WL, UK

25 <sup>5</sup>Division of Evolution and Genomic Sciences, School of Biological Sciences, University of  
26 Manchester, M13 9NT, UK

27 <sup>6</sup>HudsonAlpha Institute for Biotechnology, Huntsville AL, 35806 USA

28 <sup>7</sup>Department of Medical Genetics, Oslo University Hospital, 0424 Oslo, Norway

29 <sup>8</sup>Victorian Clinical Genetics Services, Flemington Road, Parkville, Victoria 3052, Australia

30 <sup>9</sup>Murdoch Children's Research Institute, Flemington Road, Parkville, Victoria 3052, Australia

31 <sup>10</sup>Department of Paediatrics, University of Melbourne, Royal Children's Hospital, Flemington  
32 Road, Parkville, Victoria 3052, Australia

33 <sup>11</sup>Seattle Children's, Seattle, WA 98105, USA

34 <sup>12</sup>Department of Genetics, Pitié-Salpêtrière Hospital, Assistance Publique - Hôpitaux de Paris,  
35 Groupe de Recherche Clinique Déficience Intellectuelle et Autisme UPMC, Paris 75013,  
36 France

37 <sup>13</sup>Research Centre for Medical Genetics, Moscow, 115522, Russia

38 <sup>14</sup>Max Planck Institute for Molecular Genetics, Berlin, 14195, Germany

39 <sup>15</sup>Institute for Medical and Human Genetics, Charité Universitätsmedizin Berlin, Berlin,  
40 10117, Germany

41 <sup>16</sup>Department of Medical Sciences, University of Torino, Torino, 10126 Italy

42 <sup>17</sup>Medical Genetics Unit, Città della Salute e della Scienza University Hospital, Torino,  
43 10126, Italy

44 <sup>18</sup>Department of Neurology, University of Alabama at Birmingham, Birmingham, AL 35294  
45 USA

46 <sup>19</sup>Department of Translational Medicine, Section of Pediatrics, Federico II University, Naples,  
47 80131, Italy

48 <sup>20</sup>Division of Genetics, Birth Defects & Metabolism, Ann & Robert H. Lurie Children's  
49 Hospital of Chicago, Chicago, IL 60611, USA

50 <sup>21</sup>Genetics Department, Lyon University Hospital, Lyon, 69007, France

51 <sup>22</sup>Swiss Institute of Bioinformatics (SIB), Lausanne, CH-1015, Switzerland

52 <sup>23</sup>Department of Medical Genetics, Telemark Hospital Trust, 3710 Skien, Norway

53 <sup>24</sup>Department of Genetics, University of Alabama at Birmingham, Birmingham, AL, 35233,  
54 USA

55 <sup>25</sup>New York Medical College, Valhalla, NY 10595, USA

56 <sup>26</sup>Department of Radiology, Oslo University Hospital, 0424 Oslo, Norway

57 <sup>27</sup>Integris Pediatric Neurology, Oklahoma City, OK 73112, USA

58 <sup>28</sup>Institute for Maternal and Child Health - IRCCS Burlo Garofolo, Trieste, 34100, Italy

59 <sup>29</sup>Center for Medical Genetics, Department of Pediatrics, Keio University School of  
60 Medicine, Tokyo, 1608582, Japan

61 <sup>30</sup>Department of Pediatrics, Columbia University, New York, NY 10032, USA

62 <sup>31</sup>Department of Medicine, Columbia University, New York, NY 10032, USA

63 <sup>32</sup>Institut de Génétique et de Biologie Moléculaire et Cellulaire, Illkirch, 67404, France

64 <sup>33</sup>Telethon Institute of Genetics and Medicine (TIGEM), Pozzuoli, Naples, 80078, Italy

65

66 **Correspondence should be addressed to:**

67 Alexandre Reymond, [alexandre.reymond@unil.ch](mailto:alexandre.reymond@unil.ch)

68

69 **Running title:** AFF3 degron variants

70 **Keywords:** mesomelic dysplasia, horseshoe kidney, intellectual disability, AFF3, AFF4

71

72 **Abstract**

73 The ALF transcription factor paralogs, *AFF1*, *AFF2*, *AFF3* and *AFF4*, are components of the  
74 transcriptional super elongation complex that regulates expression of genes involved in  
75 neurogenesis and development. We describe a new autosomal dominant disorder associated  
76 with *de novo* missense variants in the degron of *AFF3*, a nine amino acid sequence important  
77 for its degradation. Consistent with a causative role of *AFF3* variants, the mutated *AFF3*  
78 proteins show reduced clearance. Ten affected individuals were identified, and present with a  
79 recognizable pattern of anomalies, which we named KINSSHIP syndrome (KI for horseshoe  
80 KIdney, NS for Nievergelt/Savarirayan type of mesomelic dysplasia, S for Seizures, H for  
81 Hypertrichosis, I for Intellectual disability and P for Pulmonary involvement), partially  
82 overlapping the *AFF4* associated CHOPS syndrome. An eleventh individual with a  
83 microdeletion encompassing only the transactivation domain and degron motif of *AFF3*  
84 exhibited overlapping clinical features. A zebrafish overexpression model that shows body  
85 axis anomalies provides further support for the pathological effect of increased amount of  
86 *AFF3* protein.

87 Whereas homozygous *Aff3* knockout mice display skeletal anomalies, kidney defects, brain  
88 malformation and neurological anomalies, knock-in animals modeling the microdeletion and  
89 the missense variants identified in affected individuals presented with lower mesomelic limb  
90 deformities and early lethality, respectively.

91

92 Transcriptome analyses as well as the partial phenotypic overlap of syndromes associated  
93 with *AFF3* and *AFF4* variants suggest that ALF transcription factors are not redundant in  
94 contrast to what was previously suggested

95

## 96 **Introduction**

97

98 The *AFF1* (AF4/FMR2 family member 1, a.k.a AF4), *AFF2* (a.k.a *FMR2*), *AFF3* (a.k.a  
99 *LAF4*) and *AFF4* genes encode members of the ALF (AF4/LAF4/FMR2) family. These  
100 transcription factors share five highly conserved domains starting from the amino terminus:  
101 (i) an N-terminal homology domain (NHD); (ii) the hallmark ALF domain, which interacts  
102 with Seven In Absentia Homolog (SIAH) ubiquitin ligases through the [xPxAxVxPx] degron  
103 motif<sup>1,2</sup> and thus regulates protein degradation mediated by the proteasome pathway; (iii) a  
104 serine-rich transactivation domain<sup>3</sup>; (iv) a bipartite nuclear localization sequence (NLS); and  
105 (v) a C-terminal homology domain (CHD)<sup>4,5</sup>. *AFF1*, *AFF3*, and *AFF4* have each been  
106 identified as fusion partners of the mixed-lineage leukemia (*MLL*) gene involved in acute  
107 pediatric leukemias<sup>3</sup>. They are part of the super elongation complex<sup>6</sup> implicated in  
108 transcription of a set of genes, among them histones, retinoid signaling and *HOX* genes  
109 involved in neurogenesis and several other developmental processes (e.g. *Hoxa1*, *Cdx11* and  
110 *Cyp26a1*<sup>6,7</sup>). Mutations of the fruit fly ALF orthologous gene *lilliputian* (*lilli*) were shown to  
111 prevent neuronal differentiation and to decrease cell growth and size<sup>8,9</sup>. Silencing of *AFF2* by  
112 CGG repeat expansion is associated with FRAXE intellectual disability syndrome<sup>10</sup> (OMIM  
113 #309548), whereas hypermethylation of a mosaic CGG repeat expansion in the promoter of  
114 *AFF3*, which leads to its silencing in the central nervous system, was associated with a  
115 cytogenetic fragile site (FRA2A) and intellectual disability in three families<sup>11</sup>. *AFF3* is also  
116 known for regulating the expression of imprinted genes<sup>12,13</sup> such as *XIST* through binding to  
117 differentially methylated regions<sup>14</sup>. An individual carrying a 500kb microdeletion within the  
118 *AFF3* locus and presenting with skeletal dysplasia and encephalopathy was described<sup>15</sup>.

119

120 Six *de novo* missense variants in *AFF4* were recently linked with CHOPS (Cognitive  
121 impairment and coarse facies, Hheart defects, Obesity, Pulmonary problems, Short stature and  
122 skeletal dysplasia) syndrome<sup>16,17</sup> (OMIM#616368). They were suggested to act through  
123 reduced clearance of *AFF4* by SIAH, a hypothesis supported by the fact that surviving adult  
124 *Aff4* null mice have only azoospermia and no features of CHOPS syndrome. However, a  
125 majority of *Aff4*<sup>-/-</sup> embryos died *in utero* with severely shrunken alveoli of the lung<sup>18</sup>.  
126 Upregulation of *AFF4* resulted in dysregulation of genes involved in skeletal development  
127 and anterior/posterior pattern formation such as *MYC*, *JUN*, *TMEM100*, *ZNF711* and  
128 *FAM13C*<sup>16</sup>. These molecular changes were proposed to impair complex function and lead to

129 cohesinopathies associated with the clinical phenotypes seen in the eleven reported  
130 individuals with CHOPS and in Cornelia de Lange syndrome (CdLS; OMIM #122470)<sup>16,17</sup>.

131  
132 Here we describe 10 individuals with *de novo* missense variants in the *AFF3* gene and a  
133 recognizable pattern of anomalies including developmental delay, intellectual disability,  
134 seizures, dysmorphic facial features, mesomelic dysplasia, and failure to thrive. Although  
135 there is some overlap, the clinical presentation of this autosomal dominant disorder appears to  
136 be distinct from CHOPS syndrome.

137

## 138 **Material and Methods**

139

### 140 **Enrollment**

141 Participants were enrolled after written informed consent was obtained from parents or legal  
142 guardians according to ethical review boards policies. The clinical evaluation included  
143 medical history interviews, physical examinations and review of medical records. The  
144 Deciphering Developmental Disorders (DDD)<sup>19</sup> identifier of proband 4 is DDD276869.

145

### 146 **Exome/Genome sequencing and analysis**

147 Affected individuals were selected for sequencing to establish a diagnosis.

148 **Proband 1:** Trio exome analysis was performed on a NextSeq 500 Sequencing System  
149 (Illumina, San Diego, CA) after a 12-plex enrichment with SeqCap EZ MedExome kit  
150 (Roche, Basel, Switzerland), according to manufacturer's specifications. Sequence quality  
151 was assessed with FastQC 0.11.5, reads were mapped using BWA-MEM (v 0.7.13), sorted  
152 and indexed in a bam file (samtools 1.4.1), duplicates were flagged (sambamba 0.6.6),  
153 coverage was calculated (picard-tools 2.10.10). Variant calling was done with GATK 3.7  
154 Haplotype Caller. Variants were then annotated with SnpEff 4.3, dbNSFP 2.9.3, gnomAD,  
155 ClinVar, HGMD, and an internal database. Coverage for these samples was 93% at a 20x  
156 depth threshold.

157 **Probands 2 and 10:** Exomes were captured using the IDT xGen Exome Research Panel v1.0  
158 for proband 2 and her parents and SureSelect Human All Exon V4 (50 Mb) for proband 10  
159 and his parents. Sequencing and analyses were performed as previously described<sup>20</sup>. The  
160 general assertion criteria for variant classification are publicly available on the GeneDx  
161 ClinVar submission page.

162 **Proband 3:** The exomes of proband 3, his parents and two healthy siblings were captured and  
163 sequenced as described<sup>21</sup>. Variants were called and filtered using the Varapp software<sup>22</sup>.

164 Sanger sequencing confirmed the anticipated segregation of the potentially causative variants.

165 **Proband 4:** Exome capture and sequencing was performed as previously described<sup>19</sup>.

166 **Proband 5:** Exome sequencing of the proband was performed as previously described<sup>23</sup>.  
167 Sanger sequencing of samples from parents revealed *de novo* segregation of the variant.

168 **Proband 6:** Trio genome analysis was performed as previously described<sup>24</sup>. Sanger  
169 sequencing confirmed the *de novo* variant reported here.

170 **Proband 7:** Trio exome analysis was performed as previously described<sup>25</sup>.

171 **Proband 8:** Sample preparation and enrichment was performed using TruSeq DNA Exome  
172 kit (Illumina) and sequencing was performed using NextSeq 500 (Illumina) with mean region  
173 coverage 83x. Variant were called using VarAft software. Variant analysis was performed  
174 according to standards and guidelines for the interpretation of sequence variants<sup>26</sup>. Sanger  
175 sequencing confirmed the *de novo* origin of variant.

176 **Proband 9:** Trio exome analysis was performed with Agilent SureSelect CRE exome capture,  
177 Illumina NextSeq 500 sequencer and a mean coverage of 100x. Data were processed using  
178 Cpipe<sup>27</sup> and variant filtering and prioritization were phenotype driven (gene lists: intellectual  
179 disability, Mendeliome). Variant classification followed ACMG guidelines.

180

### 181 **Protein alignment**

182 Alignments of ALF family members were made using Clustal Omega<sup>28</sup> (v1.2.4) and imported  
183 on Jalview<sup>29</sup> for visualization.

184

### 185 **Interaction modeling**

186 3D modeling for AFF3 (UniProt entry P51826) and SIAH1 (Q8IUQ4) interaction<sup>30</sup> was  
187 obtained on Swiss-PdbViewer-DeepView<sup>31</sup> v4.1. As no structural model for human SIAH1  
188 ubiquitin-ligase was available, we used mouse ubiquitin ligase structure (pdb 2AN6) 100%  
189 conserved with human sequence in the binding region<sup>32</sup>.

190

### 191 **Mouse models**

192 Brain neuroanatomical studies were performed on three 16-week-old male mice in  
193 C57BL/6N background with homozygous knock-out of the *Aff3* (a.k.a. *Laf4*) gene<sup>33</sup>. Seventy-  
194 eight brain parameters were measured across three coronal sections as described<sup>34</sup> and data  
195 were analyzed using a mixed model and comparing to more than 100 wild-type males using a

196 false discovery rate of 1%. Other metabolic and anatomical phenotypes were assessed by the  
197 Wellcome Trust Sanger Institute through phenotyping of 6 to 13 homozygous and 7 to 14  
198 heterozygous mice and are available on the International Mouse Phenotyping Consortium  
199 website. Engineering of *Aff3*<sup>del</sup> mice model carrying a 353 kb deletion homologous to the one  
200 harbored by an affected individual<sup>15</sup> was previously published<sup>35</sup>. E18.5 animals were  
201 processed and stained as described<sup>36</sup>. With Taconic Biosciences GmbH, Cologne, Germany,  
202 we engineered a constitutive *Aff3*<sup>A233T</sup> knock-in through CRISPR/Cas9-mediated gene editing  
203 using TGGTGGATGCACGCCGGTTA as guide (NM\_001290814.1, NP\_001277743.1). This  
204 allowed the insertion of an additional silent mutation that creates an *AleI* restriction site for  
205 analytical purposes.

206

### 207 **Zebrafish overexpression model**

208 Human wild-type ORFs (*AFF3*, NM\_002285.2 and *AFF4*, NM\_014423.4) cloned into the  
209 pEZ-M13 vector were transcribed using the mMessage mMachine kit (Ambion) as prescribed.  
210 We injected 1-2 nL of diluted RNA (100-300 ng) inside the yolk, below the cell of wild-type  
211 zebrafish embryos at the 1- to 2-cell stage. Phenol red dye with distilled water was injected as  
212 vehicle control in similar volume. Injected embryos were raised at 28°C and fixed in 4% PFA  
213 for 2 hrs at 4-5 days post fertilization (dpf) and stored in PBS at 4°C. Pictures of the embryos  
214 were taken after embedding in glycerol. Counts were compared by Fisher exact test.

215

### 216 **Protein accumulation assay**

217 Tagged human wild-type mRNAs cloned into a CMV promoted expression vector were  
218 obtained from GeneCopoeia. The ORFs of *AFF3* and *AFF4* were inserted in pEZ-M13 vector  
219 with a C-terminal FLAG tag, while the ORF of *SIAH1* (NM\_001006610) was inserted in  
220 pEZ-M07 vector with a C-terminal 3xHA tag. The *AFF3* NM\_002285.2:c.697G>A,  
221 c.704T>G, and *AFF4* NM\_014423.4:c.772C>T mutations were engineered using the  
222 QuikChange II XL Site-Directed Mutagenesis Kit (Agilent Technologies) following the  
223 manufacturer's instructions. HEK293T cells cultured in complete medium (DMEM  
224 containing 10% FBS and 1% penicillin-streptomycin) were transiently transfected with wild  
225 type and mutated plasmids using calcium phosphate. 24 hrs after transfection, medium was  
226 changed to fresh complete medium. Total protein extracts were obtained after 48 hrs using  
227 RIPA buffer with protease and phosphatase inhibitor cocktail. Denatured protein extracts  
228 were immunoblotted with anti-FLAG (F3165), -HA (12CA5) and - $\beta$ -actin (A2066) antibodies  
229 from Sigma-Aldrich.



230

## 231 **Results**

232

233 We identified ten unrelated affected individuals (proband 1-10) with *de novo* missense  
234 variants in the ALF domain of AFF3 (**Figure 1A and Table 1**) through trio-based exome  
235 sequencing and data aggregation of multiple laboratories and clinical centers via  
236 GeneMatcher<sup>37</sup>. The four different identified variants (**Table 1**) (i) are not present in the  
237 Genome Aggregation Database (gnomAD<sup>38</sup> v2.1.1); (ii) are predicted to be deleterious by  
238 SIFT<sup>39</sup>, PROVEAN<sup>40</sup>, PolyPhen2<sup>41</sup> and MutationTaster2<sup>42</sup>; (iii) are part of the top 1% of all  
239 deleterious variants with CADD scores over 20; and (iv) modify highly conserved amino  
240 acids (**Figure 1B-C**). Nine of the probands present variants affecting the same codon of exon  
241 6, c.772G>T p.(A258S) (proband 1-2), c.772G>A p.(A258T) (proband 3-8), c.773C>T  
242 p.(A258V) (proband 9), whereas proband 10 carries a variant perturbing a neighboring codon  
243 c.779T>G p.(V260G) (NM\_001025108.1, NP\_001020279.1; **Table 1**). An eleventh  
244 individual (deletion proband) carrying a 500kb microdeletion and an overlapping phenotype  
245 (see below) was previously described<sup>15</sup>. This deletion removes exons 4 to 13 of *AFF3*, which  
246 encode its N-terminal region, including the ALF and its degron and part of the transactivation  
247 domains and was proposed to act as a dominant negative<sup>35</sup> (**Figure 1A**).

248

249 All *AFF3* variants described here and CHOPS syndrome-associated *AFF4 de novo* missense  
250 previously published<sup>16,17</sup> map within the degron motif of the ALF domain. This highly  
251 conserved 9 amino acid sequence [xPxAxVxPx] (**Figure 1A-B**) mediates interaction with the  
252 SIAH E3 ubiquitin ligase and regulates their degradation<sup>1</sup>. According to pathogenic variant  
253 enriched regions (PER)<sup>43</sup>, the degron is predicted to be constrained within the ALF family.  
254 Pathogenicity of the four *de novo AFF3* identified variants is further supported by the three-  
255 dimensional representation of part of the encoded peptide (**Figure 1D**). The mutated residues  
256 are located within the degron motif (KPTA<sub>258</sub>YV<sub>260</sub>RPM), which adopts a beta-strand  
257 conformation directly contacting the SIAH ubiquitin ligase binding groove<sup>30</sup>. The side chains  
258 of Alanine 258 and Valine 260 are embedded into the hydrophobic core of the beta-sandwich  
259 where the binding pockets are too small to accommodate larger side chains<sup>32</sup>. Thus, the  
260 variants p.(A258T), p.(A258S), p.(A258V) and p.(V260G) are likely to weaken or prevent  
261 binding to the ubiquitin ligase. Hence, all these *de novo* variants, as well as the 500kb deletion  
262 previously reported<sup>15</sup> that encompasses the degron, could result in hindered degradation and  
263 thus accumulation of AFF3. Consistent with this hypothesis, transiently transfected FLAG-

264 tagged  $AFF3^{A258S}$  and  $AFF3^{V260G}$  proteins were more stable than wild-type FLAG-tagged  
265  $AFF3$  (**Figure 1E**). The previously reported  $AFF4$  *de novo* variants p.(P253R), p.(T254A),  
266 p.(T254S), p.(A255T), p.(R258W) and p.(M260T) that also affect the degron motif  
267 ( $KP_{253}T_{254}A_{255}YVR_{258}PM_{260}$ ) (**Figure 1A**) were similarly shown to reduce clearance of the  
268 ALF transcription factor by SIAH<sup>16,17</sup>.

269  
270 We compared the phenotypes of the ten individuals with *de novo* variants in  $AFF3$  described  
271 here and that of the previously reported case carrying  $AFF3$  partial deletion<sup>15</sup> (**Table S1** for  
272 detailed phenotypes). They exhibit severe developmental epileptic encephalopathy (10  
273 probands out of 11), along with mesomelic dysplasia resembling Nievergelt/Savarirayan  
274 mesomelic skeletal dysplasia (NSMSD) (10/11) and failure to thrive (10/11). These three  
275 features are often associated with microcephaly (7/11), global brain atrophy and/or  
276 ventriculomegaly (7/9) (**Figure S1**), fibular hypoplasia (9/11), horseshoe kidney (8/11),  
277 abnormalities of muscle tone (9/10), gastroesophageal reflux disease (5/10) and other  
278 gastrointestinal symptoms (10/10). They also share common dysmorphic facial features such  
279 as a bulbous nasal tip (6/9), a wide mouth with square upper lip (7/10), abnormalities of the  
280 teeth and gums (9/10) and hypertrichosis (8/9) (**Figure 2-3**). Respiratory  
281 difficulties/pulmonary involvement were observed in about half of the probands with *de novo*  
282 variants (6/11). Whereas respiratory arrest led to the death of proband 3 at 21 years, the  
283 deletion proband died at four months after recurrent apneic episodes (**Table S1**).

284  
285 This constellation of features recalls some features of CHOPS-affected individuals. The three  
286 originally described probands<sup>16</sup>, along with the eight recently identified<sup>17</sup>, presented with  
287 distinctive facial dysmorphic features reminiscent of CdLS, short stature with obesity (11/11),  
288 developmental delay/intellectual disability (DD/ID) (11/11) and microcephaly (6/11) without  
289 epilepsy. They showed gastrointestinal abnormalities (8/11), accompanied by abnormal  
290 feeding behavior (6/6), hearing loss (8/11), cardiac (8/11) and pulmonary defects (8/11) and  
291 rarely horseshoe kidney (2/11). Whereas they present with vertebral abnormalities (5/11) and  
292 brachydactyly (8/11), mesomelic dysplasia is never observed and hypoplastic fibula rarely  
293 (1/11).

294  
295 Although phenotypes of  $AFF3$  and  $AFF4$  missense carriers are overlapping, they are not  
296 identical. We thus suggest naming the distinct autosomal dominant  $AFF3$ -associated disorder  
297 KINSSHIP syndrome (Kidney anomalies, Nievergelt/Savarirayan mesomelic dysplasia,

298 Seizures, Hypertrichosis and Intellectual disability with Pulmonary involvement, MIM  
299 #XXXX) to evoke both some of its cardinal characteristics, as well as its similarity (common  
300 mode of action and inheritance and overlapping phenotypes) with CHOPS syndrome.

301  
302 To better understand the functional effects of *AFF3* variation, we investigated both knock-out  
303 and knock-in mouse models (**Table 2**). We first studied the knock-out mouse line engineered  
304 by the International Mouse Phenotyping Consortium<sup>33</sup> (IMPC). The IMPC routinely measures  
305 an extensive series of parameters and evaluate if those are significantly different from wild-  
306 type mice<sup>44</sup> ( $p \leq 10^{-04}$ ). *Aff3*<sup>+/-</sup> and *Aff3*<sup>-/-</sup> mice exhibit skeletal defects including fusion of  
307 vertebral arches, vertebral transformation and decreased caudal vertebrae number.  
308 Homozygous knock-out mice also show an abnormal skull shape with a small, deviated snout  
309 and malocclusion as well as decreased serum fructosamine and albumin levels that could  
310 reflect kidney defects and/or metabolic dysregulation. Neurological dysfunctions were also  
311 noted with an increased or absent threshold for auditory brainstem response (signs of hearing  
312 impairment) and diminished grip strength. As *Aff3* is expressed in progenitor neurons<sup>45</sup> and  
313 required for neuronal migration in the cerebral cortex<sup>46</sup>, we further assessed the consequences  
314 of *Aff3* disruption on brain development by measuring a standardized set of 78 parameters  
315 across 22 brain regions<sup>34</sup>. Compared with wild type males, homozygous *Aff3*<sup>-/-</sup>, but not  
316 heterozygous *Aff3*<sup>+/-</sup> males, exhibited significantly enlarged lateral ventricles ( $p = 1.24 \times 10^{-$   
317 <sup>04</sup>) and decreased corpus callosum size ( $p = 3.02 \times 10^{-06}$ ; **Figure 4**), similar to the phenotypes  
318 observed in proband 2, 3 and 6 and in the previously reported deletion proband (**Table S1**,  
319 **Figure S1**)<sup>15</sup>. These features are in stark contrast with results obtained with another  
320 engineered *Aff3*<sup>-/-</sup> line that showed no phenotypic perturbations possibly because of genetic  
321 background differences, i.e. C57BL/6N versus CD1, and/or focusing on limb morphology  
322 only<sup>35</sup>.

323  
324 We then reassessed mouse models mimicking the deletion identified in the previously  
325 described proband, which were previously engineered to assess an aggregation method for the  
326 rapid generation of structural variants<sup>35</sup>. Consistent with the phenotype of the deletion  
327 proband, homozygous animals chimeric for a 353kb deletion syntenic to the 500kb human  
328 deletion exhibited mesomelic dysplasia, triangular tibia, severe hypoplastic fibula and  
329 polydactyly of the feet<sup>35</sup> (**Table 2**). Reexamination of these *Aff3*<sup>del/del</sup> (a.k.a. *Laf4*<sup>del/del</sup>) mice  
330 showed that they also presented with reduced body size, craniofacial dysmorphisms with  
331 delayed ossification of skull bones, hypoplastic pelvis, intestinal prolapse and neurological

332 dysfunction (**Figure 5A-C**). Chimeric *Aff3*<sup>del/+</sup> heterozygotes presented with variable features  
333 ranging from unaffected to homozygous deletion-like phenotypes. Whereas *Aff3*<sup>del/+</sup> animals  
334 with low chimerism were fertile they produced no heterozygous offspring suggesting lethality  
335 of the 353kb deletion (**Table 2**). While these results support a causative role for the deletion  
336 in the deletion proband, they do not allow differentiating between gain-of-function and  
337 haploinsufficiency.

338  
339 To further assess the underlying mutational mechanism in our missense probands, we  
340 engineered a knock-in mouse model carrying the *Aff3*<sup>A233T</sup> mutation that is the equivalent of  
341 the most commonly observed *de novo* variant, identified in probands 3 to 8 [p.(A258T)]. The  
342 microinjection of a total of 410 C57BL/6NTac zygotes and transfers into 14 recipient females  
343 to allow CRISPR/Cas9 editing resulted in only 13 pups at weaning. Genotyping showed that  
344 most of them were either wild type (8 individuals) or carried CRISPR/Cas9-mediated  
345 mutations (4) although reduced gRNA activity was used for microinjection. A single female  
346 F0 founder animal showed the targeted A233T knock-in but with a very low mosaicism rate  
347 of 16.7% in an ear biopsy. Genotyping showed that none of its offspring from four  
348 consecutive pregnancies were heterozygous for the mutation. These results suggest that the  
349 *Aff3*<sup>A233T</sup> mutation is lethal with high mosaicism (homozygous *Aff3*<sup>A233T/A233T</sup> and  
350 heterozygous *Aff3*<sup>+/A233T</sup> chimeras), in gametes or during the fetal period (heterozygous  
351 *Aff3*<sup>+/A233T</sup>; **Table 2**). The success statistics of similar CRISPR/Cas9 knock-in projects  
352 performed by Taconic Biosciences GmbH (Cologne, Germany) through the years further  
353 support this hypothesis. Out of 92 attempted knock-in constructs 98% were successful with  
354 only 2% failing to generate F0 animals. For most projects, positive F1 animals were also  
355 generated.

356  
357 To lend further support to the model centered on a pathological increase of AFF3 protein  
358 product in affected individuals, we assessed its accumulation in zebrafish. Whereas the  
359 genome of these teleosts encodes four ALF transcription factors orthologous to the  
360 mammalian *AFF1* to *AFF4*, these genes do not harbor a [xPxAxVxPx] degron motif  
361 suggesting that their degradation is regulated differently in fish. Therefore, we modeled  
362 accumulation by independently overexpressing increasing amounts of unmutated human  
363 AFF3 and AFF4 mRNA in zebrafish embryos. We observed a dose-dependent increase in the  
364 fraction of 4 dpf embryos with morphological defects upon overexpression of AFF3. The  
365 observed phenotypes included bent body axis, yolk sac edema and generalized body

366 development defects at higher doses (**Figure 5D-E**). A similar albeit less pronounced dose-  
367 dependent increase in zebrafish embryos with morphological defects was seen upon  
368 overexpression of *AFF4* (**Figure 5E**).

369  
370 To further assess the redundancy of ALF transcription factors, we took advantage of  
371 published knockdown experiments<sup>47</sup>. Luo and colleagues established and profiled the  
372 transcriptome of stable HEK293T cell lines independently knocked down for *AFF2*, *AFF3*  
373 and *AFF4* expression by specific shRNAs. Reanalysis of these data confirmed that ALF  
374 transcription factors have mostly different target genes, as 55% (125 out of 226), 62%  
375 (261/423) and 87% (966/1116) of the genes are specifically perturbed by the knock down of  
376 *AFF2*, *AFF3* and *AFF4*, respectively (**Figure 6A**). Intriguingly, the subset of common targets  
377 is similarly influenced by decreased expression of *AFF2* and *AFF3* (**Figure 6C,D**), whereas  
378 knocking down *AFF3* and *AFF4* had opposite effect (**Figure 6B,C**). 95% (119 out of 125) of  
379 common targets are decreased upon reduction of *AFF3* and increased upon reduction of *AFF4*  
380 expression suggesting that these two transcription factors act as positive and negative  
381 regulators of common pathways. Within the genes perturbed by both *AFF3* and *AFF4*, we  
382 observed a significant overrepresentation of genes implicated in the gastrin hormone pathway  
383 (CCKR signaling map, P06959) and a proton pump complex (vacuolar proton-transporting V-  
384 type ATPase complex, GO:0016471) possibly associated with the gastroesophageal reflux  
385 disease observed in both KINSSHIP and CHOPS individuals. Genes linked to the  
386 gonadotropin-releasing hormone receptor pathway are similarly enriched (P06664). This  
387 observation could be related to cryptorchidism of KINSSHIP proband 1 and small  
388 genitalia/cryptorchidism in three out of five males affected by CHOPS syndrome<sup>16,17</sup>, as well  
389 as the erratic menstrual cycle of proband 4 (most probands being too young to predict any  
390 pubertal anomaly) and popliteal pterygium in proband 8 (**Table S1**).

## 391 392 **Discussion**

393 All eleven individuals with an *AFF3* variant we identified have a complex but overlapping  
394 clinical presentation, which we named KINSSHIP syndrome. One of the cardinal  
395 characteristics of this rare autosomal dominant syndrome is mesomelic dysplasia with short  
396 forearms, radial head dislocation/subluxation, triangular and/or short tibia, fibular hemimelia,  
397 hip dislocation, tarsal and/or metatarsal synostosis resembling NSMSD (**Figure 3**). NSMSD  
398 is a sporadic or rare autosomal dominant condition<sup>48,49</sup> associated with neurodevelopmental  
399 and often urogenital abnormalities<sup>50,51</sup>. KINSSHIP affected individuals similarly present with

400 vertebral and bone mineralization defects, scoliosis, epilepsy, severe global DD/ID sometimes  
401 associated with structural brain abnormalities, significant feeding difficulties, horseshoe  
402 kidney, hypertrichosis and recognizable facial features. Multiple probands showed coarsening  
403 facial features with age, including a large nose with bulbous nasal tip, a prominent columella  
404 and a wide mouth with square upper lip (**Figure 2-3, Table S1, Figure S1**).

405  
406 *AFF3* is one of the targets of the Wnt/ $\beta$ -catenin pathway, an important contributor to  
407 pathways involved in bone development and homeostasis<sup>52,53</sup>. Variants in *WNT* genes cause a  
408 diverse range of skeletal dysplasias including mesomelic defects (*WNT5A*; Robinow  
409 syndrome, dominant type, OMIM#180700), decreased bone density (*WNT1*; Osteogenesis  
410 imperfecta, type XV, OMIM#615220) and limb hypoplasia–reduction defects including  
411 fibular a/hypoplasia (*WNT3* and *WNT7A*; Tetra-amelia OMIM#273395 and Fuhrmann  
412 syndrome OMIM#228930, respectively). Of note individuals with Robinow rhizo/mesomelic  
413 dysplasia also present with developmental kidney abnormalities<sup>54</sup>, whereas perturbations of  
414 the Wnt/ $\beta$ -catenin pathway have been associated with the development of ectodermal  
415 appendages like hair and teeth<sup>55</sup>. Nine out of ten KINSSHIP probands show dental anomalies.  
416 While widespread hypertrichosis may have been partially caused by multi-drug, antiepileptic  
417 treatment in probands 3 and 4, its presence in the only non-epileptic *AFF3* individual  
418 (proband 9) and the much younger proband 5 seems to confirm the association of this feature  
419 with *AFF3* genetic variants. It is possible that the complex clinical presentation of the cases  
420 described here (**Table S1**) may represent the effects of impaired *AFF3* function on a number  
421 of downstream targets within the Wnt/ $\beta$ -catenin pathway. In-depth transcriptome analysis of  
422 affected individuals and/or animal models is warranted to confirm this hypothesis.

423  
424 Despite the limited number of individuals for both conditions, similarities and differences are  
425 notable between individuals with KINSSHIP and CHOPS<sup>16,17</sup> syndrome. Individuals with  
426 variants in *AFF3* and *AFF4* share features that include respiratory difficulties and vertebral  
427 abnormalities, as well as less specific clinical findings such as microcephaly, DD/ID and  
428 gastroesophageal reflux disease. Although skeletal abnormalities are reported in both CHOPS  
429 and KINSSHIP syndrome, KINSSHIP individuals present with mesomelic dysplasia, whereas  
430 CHOPS individuals show brachydactyly. Seizures and failure to thrive are specific to  
431 KINSSHIP and obesity with short stature to CHOPS. Congenital heart defects and hearing  
432 loss are typically observed in CHOPS, while horseshoe kidney and hypoplastic fibula are  
433 predominantly present in KINSSHIP (80% versus 18% and 80% versus 9% of affected

434 individuals, respectively). Despite having thick hair and coarse facies in common, CHOPS  
435 probands differ from KINSSHIP probands by their round face and dysmorphic features  
436 resembling those of CdLS individuals<sup>16,17</sup>.

437  
438 Although proteins encoded by *AFF2*, *AFF3* and *AFF4* were reported to be functionally  
439 redundant, at least in regulating splicing and transcription during normal brain development<sup>56</sup>,  
440 the clinically distinct phenotypes of individuals carrying *de novo* variants in the degron of  
441 *AFF3* and *AFF4* and our zebrafish results suggest that the encoded proteins are not fully  
442 redundant. Further support for this hypothesis is provided by the intolerance to LoF variant of  
443 *AFF1* (pLI=0.8), *AFF2* (pLI=1), *AFF3* (pLI=1) and *AFF4* (pLI=1) reported by GnomAD.  
444 Whereas homozygous *Aff3*<sup>-/-</sup> knockout mice display features comparable to those presented by  
445 KINSSHIP individuals such as skeletal anomalies, kidney defects, brain malformations and  
446 neurological anomalies, these animals do not recapitulate the characteristic mesomelia  
447 contrary to *Aff3*<sup>del/del</sup> mice model. This result and the aforementioned intolerance to LoF  
448 suggest that *AFF3* could be associated with two different syndromes, the one described here  
449 caused by missense degron variants and a hemizygous deletion of the degron, as well as a  
450 second one associated with LoF variants for which affected humans remain to be identified.  
451 Although this hypothesis warrants further investigation, we have identified by exome  
452 sequencing an individual with features partially overlapping those of KINSSHIP. He is  
453 compound heterozygote for a truncating mutation and a predicted to be deleterious missense  
454 variant outside of the degron.

455  
456 In conclusion we describe a new pathology that we propose to name KINSSHIP syndrome. It  
457 is associated with variants in the degron of *AFF3* that affect the degradation of the encoded  
458 protein. This syndrome shows similarities with the *AFF4*-associated CHOPS syndrome, in  
459 particular its gain of protein stability and affected tissues. However, specific KINSSHIP  
460 features such as mesomelic dysplasia combined with horseshoe kidney allow a differential  
461 diagnosis.

462

463 **Supplemental Data**

464 Supplemental data include 1 figure and 1 table.

465 Figure S1: Brain MRI of proband 7 carrying a de novo variant in AFF3

466 Table S1: Phenotype of individuals with AFF3 variants

467

468 **Conflicts of Interests**

469 Tara Funari, Ganka Douglas, Jane Juusola, and Rhonda E. Schnur and Wendy K. Chung are  
470 employees and former employees of GeneDx, respectively. The remaining authors declare  
471 that they have no competing interests.

472

473 **Acknowledgments**

474 We thank the probands and their families for their participation in this study. We are grateful  
475 to Jacques S. Beckmann, Giedre Grigelioniene and the Genomic Technologies Facility of the  
476 University of Lausanne. This work was supported by grants from the Swiss National Science  
477 Foundation (31003A\_182632 to AR), the Simons Foundation (SFARI274424 to AR and  
478 SFARI337701 to WKC) and NHGRI (grant UMIHG007301 to SMH, EMB, GMC). The  
479 DDD study presents independent research commissioned by the Health Innovation Challenge  
480 Fund [grant number HICF-1009-003], a parallel funding partnership between Wellcome and  
481 the Department of Health, and the Wellcome Sanger Institute [grant number WT098051]. The  
482 views expressed in this publication are those of the author(s) and not necessarily those of  
483 Wellcome or the Department of Health. The study has UK Research Ethics Committee  
484 approval (10/H0305/83, granted by the Cambridge South REC, and GEN/284/12 granted by  
485 the Republic of Ireland REC). The research team acknowledges the support of the National  
486 Institute for Health Research, through the Comprehensive Clinical Research Network. This  
487 study makes use of DECIPHER which is funded by the Wellcome. We acknowledge the  
488 Sanger Mouse Genetics Project for providing mouse samples, funded by the Wellcome Trust  
489 grant number 098051. The Australian National Health & Medical Research Council  
490 (NHMRC) provided funding for sequencing proband 9 under the Australian Genomics Health  
491 Alliance (GNT1113531); the contents are solely the responsibility of the individual authors  
492 and do not reflect the views of the NHMRC. The research conducted at the Murdoch  
493 Children's Research Institute was supported by the Victorian Government's Operational  
494 Infrastructure Support Program. The funders had no role in study design, data collection and  
495 analysis, decision to publish, or preparation of the manuscript.

496



497 **Web Resources**

- 498 ClustalOmega: <http://www.clustal.org/omega/>  
499 DDD: <http://www.ddduk.org/>  
500 GeneMatcher: <https://genematcher.org/>  
501 GeneDx ClinVar submission page: <http://www.ncbi.nlm.nih.gov/clinvar/submitters/26957/>  
502 GnomAD: <https://gnomad.broadinstitute.org/about>.  
503 IMPC: <http://www.mousephenotype.org/>  
504 MutationTaster2: <http://www.mutationtaster.org/>  
505 PANTHER: <http://www.pantherdb.org>  
506 PER viewer: <http://per.broadinstitute.org/>  
507 PolyPhen-2: <http://genetics.bwh.harvard.edu/pph2/index.shtml>  
508 PROVEAN: <http://provean.jcvi.org/index.php>  
509 SIFT: <http://sift.jcvi.org/>  
510 Varaft: <https://varaft.eu>  
511 Varapp: <https://varapp-demo.vital-it.ch>

512  
513  
514  
515  
516  
517  
518  
519  
520  
521  
522  
523  
524  
525  
526  
527  
528  
529  
530  
531  
532  
533  
534  
535  
536  
537  
538  
539  
540  
541  
542  
543  
544  
545  
546  
547  
548  
549  
550  
551  
552  
553  
554  
555  
556  
557  
558  
559

## References

1. House, C.M., Frew, I.J., Huang, H.L., Wiche, G., Traficante, N., Nice, E., Catimel, B., and Bowtell, D.D. (2003). A binding motif for Siah ubiquitin ligase. *Proc Natl Acad Sci U S A* 100, 3101-3106.
2. Bitoun, E., and Davies, K.E. (2005). The robotic mouse: unravelling the function of AF4 in the cerebellum. *Cerebellum* 4, 250-260.
3. Meyer, C., Hofmann, J., Burmeister, T., Groger, D., Park, T.S., Emerenciano, M., Pombo de Oliveira, M., Renneville, A., Villarese, P., Macintyre, E., et al. (2013). The MLL recombinome of acute leukemias in 2013. *Leukemia* 27, 2165-2176.
4. Nilson, I., Reichel, M., Ennas, M.G., Greim, R., Knorr, C., Siegler, G., Greil, J., Fey, G.H., and Marschalek, R. (1997). Exon/intron structure of the human AF-4 gene, a member of the AF-4/LAF-4/FMR-2 gene family coding for a nuclear protein with structural alterations in acute leukaemia. *Br J Haematol* 98, 157-169.
5. Oliver, P.L., Bitoun, E., Clark, J., Jones, E.L., and Davies, K.E. (2004). Mediation of Af4 protein function in the cerebellum by Siah proteins. *Proc Natl Acad Sci U S A* 101, 14901-14906.
6. Luo, Z., Lin, C., and Shilatifard, A. (2012). The super elongation complex (SEC) family in transcriptional control. *Nat Rev Mol Cell Biol* 13, 543-547.
7. Jonkers, I., and Lis, J.T. (2015). Getting up to speed with transcription elongation by RNA polymerase II. *Nat Rev Mol Cell Biol* 16, 167-177.
8. Tang, A.H., Neufeld, T.P., Rubin, G.M., and Muller, H.A. (2001). Transcriptional regulation of cytoskeletal functions and segmentation by a novel maternal pair-rule gene, lilliputian. *Development* 128, 801-813.
9. Wittwer, F., van der Straten, A., Keleman, K., Dickson, B.J., and Hafen, E. (2001). Lilliputian: an AF4/FMR2-related protein that controls cell identity and cell growth. *Development* 128, 791-800.
10. Geetz, J., Gedeon, A.K., Sutherland, G.R., and Mulley, J.C. (1996). Identification of the gene FMR2, associated with FRAXE mental retardation. *Nat Genet* 13, 105-108.
11. Metsu, S., Rooms, L., Rainger, J., Taylor, M.S., Bengani, H., Wilson, D.I., Chilamakuri, C.S., Morrison, H., Vandeweyer, G., Reyniers, E., et al. (2014). FRA2A is a CGG repeat expansion associated with silencing of AFF3. *PLoS Genet* 10, e1004242.
12. Luo, Z., Lin, C., Woodfin, A.R., Bartom, E.T., Gao, X., Smith, E.R., and Shilatifard, A. (2016). Regulation of the imprinted Dlk1-Dio3 locus by allele-specific enhancer activity. *Genes Dev* 30, 92-101.
13. Wang, Y., Shen, Y., Dai, Q., Yang, Q., Zhang, Y., Wang, X., Xie, W., Luo, Z., and Lin, C. (2017). A permissive chromatin state regulated by ZFP281-AFF3 in controlling the imprinted Meg3 polycistron. *Nucleic Acids Res* 45, 1177-1185.
14. Zhang, Y., Wang, C., Liu, X., Yang, Q., Ji, H., Yang, M., Xu, M., Zhou, Y., Xie, W., Luo, Z., et al. (2018). AFF3-DNA methylation interplay in maintaining the mono-allelic expression pattern of XIST in terminally differentiated cells. *J Mol Cell Biol*.
15. Steichen-Gersdorf, E., Gassner, I., Superti-Furga, A., Ullmann, R., Stricker, S., Klopocki, E., and Mundlos, S. (2008). Triangular tibia with fibular aplasia associated with a microdeletion on 2q11.2 encompassing LAF4. *Clin Genet* 74, 560-565.
16. Izumi, K., Nakato, R., Zhang, Z., Edmondson, A.C., Noon, S., Dulik, M.C., Rajagopalan, R., Venditti, C.P., Gripp, K., Samanich, J., et al. (2015). Germline gain-of-function mutations in AFF4 cause a developmental syndrome functionally linking the super elongation complex and cohesin. *Nat Genet* 47, 338-344.

- 560 17. Raible, S.E., Mehta, D., Bettale, C., Fiordaliso, S., Kaur, M., Medne, L., Rio, M., Haan,  
561 E., White, S.M., Cusmano-Ozog, K., et al. (2019). Clinical and molecular spectrum of  
562 CHOPS syndrome. *Am J Med Genet A*.
- 563 18. Urano, A., Endoh, M., Wada, T., Morikawa, Y., Itoh, M., Kataoka, Y., Taki, T., Akazawa,  
564 H., Nakajima, H., Komuro, I., et al. (2005). Infertility with defective spermiogenesis  
565 in mice lacking AF5q31, the target of chromosomal translocation in human infant  
566 leukemia. *Mol Cell Biol* 25, 6834-6845.
- 567 19. Deciphering Developmental Disorders, S. (2015). Large-scale discovery of novel genetic  
568 causes of developmental disorders. *Nature* 519, 223-228.
- 569 20. Retterer, K., Juusola, J., Cho, M.T., Vitazka, P., Millan, F., Gibellini, F., Vertino-Bell, A.,  
570 Smaoui, N., Neidich, J., Monaghan, K.G., et al. (2016). Clinical application of whole-  
571 exome sequencing across clinical indications. *Genet Med* 18, 696-704.
- 572 21. Alfaiz, A.A., Micale, L., Mandriani, B., Augello, B., Pellico, M.T., Chrast, J., Xenarios, I.,  
573 Zelante, L., Merla, G., and Reymond, A. (2014). TBC1D7 mutations are associated  
574 with intellectual disability, macrocrania, patellar dislocation, and celiac disease. *Hum*  
575 *Mutat* 35, 447-451.
- 576 22. Delafontaine J., M.A., Liechti R., Kuznetsov D., Xenarios I., Pradervand S. (2016).  
577 Varapp: A reactive web-application for variants filtering. bioRxiv preprint.
- 578 23. Holla, O.L., Bock, G., Busk, O.L., and Isfoss, B.L. (2014). Familial visceral myopathy  
579 diagnosed by exome sequencing of a patient with chronic intestinal pseudo-  
580 obstruction. *Endoscopy* 46, 533-537.
- 581 24. Bowling, K.M., Thompson, M.L., Amaral, M.D., Finnila, C.R., Hiatt, S.M., Engel, K.L.,  
582 Cochran, J.N., Brothers, K.B., East, K.M., Gray, D.E., et al. (2017). Genomic  
583 diagnosis for children with intellectual disability and/or developmental delay. *Genome*  
584 *Med* 9, 43.
- 585 25. Takenouchi, T., Yamaguchi, Y., Tanikawa, A., Kosaki, R., Okano, H., and Kosaki, K.  
586 (2015). Novel overgrowth syndrome phenotype due to recurrent de novo PDGFRB  
587 mutation. *J Pediatr* 166, 483-486.
- 588 26. Richards, S., Aziz, N., Bale, S., Bick, D., Das, S., Gastier-Foster, J., Grody, W.W., Hegde,  
589 M., Lyon, E., Spector, E., et al. (2015). Standards and guidelines for the interpretation  
590 of sequence variants: a joint consensus recommendation of the American College of  
591 Medical Genetics and Genomics and the Association for Molecular Pathology. *Genet*  
592 *Med* 17, 405-424.
- 593 27. Sadedin, S.P., Dashnow, H., James, P.A., Bahlo, M., Bauer, D.C., Lonie, A., Lunke, S.,  
594 Macciocca, I., Ross, J.P., Siemering, K.R., et al. (2015). Cpipe: a shared variant  
595 detection pipeline designed for diagnostic settings. *Genome Med* 7, 68.
- 596 28. Sievers, F., Wilm, A., Dineen, D., Gibson, T.J., Karplus, K., Li, W., Lopez, R.,  
597 McWilliam, H., Remmert, M., Soding, J., et al. (2011). Fast, scalable generation of  
598 high-quality protein multiple sequence alignments using Clustal Omega. *Mol Syst*  
599 *Biol* 7, 539.
- 600 29. Waterhouse, A.M., Martin, D.M.A., Barton, G.J., Procter, J.B., and Clamp, M. (2009).  
601 Jalview Version 2—a multiple sequence alignment editor and analysis workbench.  
602 *Bioinformatics* 25, 1189-1191.
- 603 30. Santelli, E., Leone, M., Li, C., Fukushima, T., Preece, N.E., Olson, A.J., Ely, K.R., Reed,  
604 J.C., Pellecchia, M., Liddington, R.C., et al. (2005). Structural analysis of Siah1-Siah-  
605 interacting protein interactions and insights into the assembly of an E3 ligase  
606 multiprotein complex. *J Biol Chem* 280, 34278-34287.
- 607 31. Johansson, M.U., Zoete, V., Michielin, O., and Guex, N. (2012). Defining and searching  
608 for structural motifs using DeepView/Swiss-PdbViewer. *BMC Bioinformatics* 13,  
609 173.

- 610 32. House, C.M., Hancock, N.C., Moller, A., Cromer, B.A., Fedorov, V., Bowtell, D.D.,  
611 Parker, M.W., and Polekhina, G. (2006). Elucidation of the substrate binding site of  
612 Siah ubiquitin ligase. *Structure* 14, 695-701.
- 613 33. Skarnes, W.C., Rosen, B., West, A.P., Koutsourakis, M., Bushell, W., Iyer, V., Mujica,  
614 A.O., Thomas, M., Harrow, J., Cox, T., et al. (2011). A conditional knockout resource  
615 for the genome-wide study of mouse gene function. *Nature* 474, 337-342.
- 616 34. Mikhaleva, A., Kannan, M., Wagner, C., and Yalcin, B. (2016). Histomorphological  
617 Phenotyping of the Adult Mouse Brain. *Curr Protoc Mouse Biol* 6, 307-332.
- 618 35. Kraft, K., Geuer, S., Will, A.J., Chan, W.L., Paliou, C., Borschiwer, M., Harabula, I.,  
619 Wittler, L., Franke, M., Ibrahim, D.M., et al. (2015). Deletions, Inversions,  
620 Duplications: Engineering of Structural Variants using CRISPR/Cas in Mice. *Cell Rep*  
621 10, 833-839.
- 622 36. Mundlos, S. (2000). Skeletal morphogenesis. *Methods Mol Biol* 136, 61-70.
- 623 37. Sobreira, N., Schiettecatte, F., Valle, D., and Hamosh, A. (2015). GeneMatcher: a  
624 matching tool for connecting investigators with an interest in the same gene. *Hum*  
625 *Mutat* 36, 928-930.
- 626 38. Karczewski, K.J., Francioli, L.C., Tiao, G., Cummings, B.B., Alföldi, J., Wang, Q.,  
627 Collins, R.L., Laricchia, K.M., Ganna, A., Birnbaum, D.P., et al. (2019). Variation  
628 across 141,456 human exomes and genomes reveals the spectrum of loss-of-function  
629 intolerance across human protein-coding genes. *bioRxiv*, 531210.
- 630 39. Kumar, P., Henikoff, S., and Ng, P.C. (2009). Predicting the effects of coding non-  
631 synonymous variants on protein function using the SIFT algorithm. *Nat Protoc* 4,  
632 1073-1081.
- 633 40. Choi, Y., and Chan, A.P. (2015). PROVEAN web server: a tool to predict the functional  
634 effect of amino acid substitutions and indels. *Bioinformatics* 31, 2745-2747.
- 635 41. Adzhubei, I.A., Schmidt, S., Peshkin, L., Ramensky, V.E., Gerasimova, A., Bork, P.,  
636 Kondrashov, A.S., and Sunyaev, S.R. (2010). A method and server for predicting  
637 damaging missense mutations. *Nat Methods* 7, 248-249.
- 638 42. Schwarz, J.M., Cooper, D.N., Schuelke, M., and Seelow, D. (2014). MutationTaster2:  
639 mutation prediction for the deep-sequencing age. *Nature Methods* 11, 361.
- 640 43. Pérez-Palma, E., May, P., Iqbal, S., Niestroj, L.-M., Du, J., Heyne, H., Castrillon, J.,  
641 O'Donnell-Luria, A., Nürnberg, P., Palotie, A., et al. (2019). Identification of  
642 pathogenic variant enriched regions across genes and gene families. *bioRxiv*, 641043.
- 643 44. Brown, S.D., and Moore, M.W. (2012). The International Mouse Phenotyping  
644 Consortium: past and future perspectives on mouse phenotyping. *Mamm Genome* 23,  
645 632-640.
- 646 45. Fietz, S.A., Lachmann, R., Brandl, H., Kircher, M., Samusik, N., Schroder, R.,  
647 Lakshmanaperumal, N., Henry, I., Vogt, J., Riehn, A., et al. (2012). Transcriptomes of  
648 germinal zones of human and mouse fetal neocortex suggest a role of extracellular  
649 matrix in progenitor self-renewal. *Proc Natl Acad Sci U S A* 109, 11836-11841.
- 650 46. Moore, J.M., Oliver, P.L., Finelli, M.J., Lee, S., Lickiss, T., Molnar, Z., and Davies, K.E.  
651 (2014). *Laf4/Aff3*, a gene involved in intellectual disability, is required for cellular  
652 migration in the mouse cerebral cortex. *PLoS One* 9, e105933.
- 653 47. Luo, Z., Lin, C., Guest, E., Garrett, A.S., Mohaghegh, N., Swanson, S., Marshall, S.,  
654 Florens, L., Washburn, M.P., and Shilatifard, A. (2012). The super elongation  
655 complex family of RNA polymerase II elongation factors: gene target specificity and  
656 transcriptional output. *Mol Cell Biol* 32, 2608-2617.
- 657 48. Nakamura, M., Matsuda, Y., Higo, M., and Nishimura, G. (2007). A family with an  
658 autosomal dominant mesomelic dysplasia resembling mesomelic dysplasia  
659 Savarirayan and Nievergelt types. *Am J Med Genet A* 143A, 2079-2081.

- 660 49. Bonafe, L., Cormier-Daire, V., Hall, C., Lachman, R., Mortier, G., Mundlos, S.,  
661 Nishimura, G., Sangiorgi, L., Savarirayan, R., Sillence, D., et al. (2015). Nosology and  
662 classification of genetic skeletal disorders: 2015 revision. *Am J Med Genet A* 167A,  
663 2869-2892.
- 664 50. Tuysuz, B., Zeybek, C., Zorer, G., Sipahi, O., and Ungur, S. (2002). Patient with the  
665 mesomelic dysplasia, Nievergelt syndrome, and cerebellovermian agenesis and  
666 cataracts. *Am J Med Genet* 109, 206-210.
- 667 51. Savarirayan, R., Cormier-Daire, V., Curry, C.J., Nashelsky, M.B., Rappaport, V., Rimoin,  
668 D.L., and Lachman, R.S. (2000). New mesomelic dysplasia with absent fibulae and  
669 triangular tibiae. *Am J Med Genet* 94, 59-63.
- 670 52. Lefevre, L., Omeiri, H., Drougat, L., Hantel, C., Giraud, M., Val, P., Rodriguez, S.,  
671 Perlemoine, K., Blugeon, C., Beuschlein, F., et al. (2015). Combined transcriptome  
672 studies identify *AFF3* as a mediator of the oncogenic effects of beta-catenin in  
673 adrenocortical carcinoma. *Oncogenesis* 4, e161.
- 674 53. Zhong, Z., Ethen, N.J., and Williams, B.O. (2014). WNT signaling in bone development  
675 and homeostasis. *Wiley Interdiscip Rev Dev Biol* 3, 489-500.
- 676 54. Tufan, F., Cefle, K., Turkmen, S., Turkmen, A., Zorba, U., Dursun, M., Ozturk, S.,  
677 Palanduz, S., Eceder, T., Mundlos, S., et al. (2005). Clinical and molecular  
678 characterization of two adults with autosomal recessive Robinow syndrome. *Am J*  
679 *Med Genet A* 136, 185-189.
- 680 55. Kimura, R., Watanabe, C., Kawaguchi, A., Kim, Y.I., Park, S.B., Maki, K., Ishida, H., and  
681 Yamaguchi, T. (2015). Common polymorphisms in *WNT10A* affect tooth  
682 morphology as well as hair shape. *Hum Mol Genet* 24, 2673-2680.
- 683 56. Melko, M., Douguet, D., Bensaïd, M., Zongaro, S., Verheggen, C., Gecz, J., and Bardoni,  
684 B. (2011). Functional characterization of the *AFF* (*AF4/FMR2*) family of RNA-  
685 binding proteins: insights into the molecular pathology of *FRAXE* intellectual  
686 disability. *Hum Mol Genet* 20, 1873-1885.
- 687

## 688 **Figure Titles and Legends**

689

### 690 **Figure 1: AFF3 and AFF4 degron motif variants**

691 **(A)** Schematic protein structure of ALF proteins with from the amino terminus a N-terminal  
692 homology domain (NHD), the AF4/LAF4/FMR2 homology domain (ALF)<sup>21</sup> containing the  
693 SIAH-binding degron motif, a serine-rich transactivation domain (TAD)<sup>3</sup>, a bipartite  
694 nuclear/nucleolar localization sequence (NLS), and a C-terminal homology domain (CHD).  
695 The sequences of the degron motif of AFF3 and AFF4 are shown above. The residues  
696 modified in the KINSSHIP probands described in this manuscript and individuals affected by  
697 CHOPS<sup>16,17</sup> are highlighted in bold and numbered. The extent of the 500kb deletion  
698 previously described<sup>35</sup> is indicated here. A red arrow pinpoints the position of the degron  
699 motif.

700 **(B)** Amino acid sequences alignment of human AFF1, AFF2, AFF3 and AFF4 proteins  
701 (ENSP00000305689, ENSP00000359489, ENSP00000317421 and ENSP00000265343,  
702 respectively) showing the highly conserved degron motif (red rectangle) of the ALF  
703 homology domain that provides the binding moiety to the SIAH ubiquitin-ligase. Sequences  
704 alignment was performed using Clustal Omega and edited using Jalview. Shading is  
705 proportional to conservation among sequences.

706 **(C)** Amino acid sequences alignment of different AFF3 vertebrate orthologs showing the  
707 conservation of the degron motif (red rectangle). Accession numbers are ENSP00000317421  
708 (human), ENSMUSP00000092637 (mouse), ENSFCAP00000024603 (cat),  
709 ENSLAFP00000010776 (elephant), ENSPSIP00000007060 (chinese turtle),  
710 ENSACAP00000008035 (anole lizard) and ENSPMAP00000008605 (lamprey).

711 **(D)** 3D modeling of the binding of human AFF3 degron to the mouse Siah ubiquitin ligase.  
712 PDB entry 2AN6<sup>32</sup> was loaded in Swiss-PdbViewer<sup>31</sup> and used as a template to align the  
713 human SIAH ubiquitin ligase (uniprot entry Q8IUQ4)<sup>30</sup>. With respect to the mouse crystal  
714 structure, the only difference is the presence of an aspartic acid residue instead of a glutamic  
715 acid at position 116. The region of AFF3 containing the degron motif (LRPVAMVRPTV)  
716 was then aligned onto the Siah-interacting protein<sup>50</sup> peptide present in the crystal structure  
717 (QKPTAYVRPMD) to highlight the position of the variants reported in this study. For clarity,  
718 only side-chains of the core degron motif (P256, A258, V260 and P262) are shown, with  
719 yellow highlights on the KINSSHIP mutated residues. A zoom in is displayed on the right.  
720 The core degron motif adopts a beta-strand conformation directly contacting the ubiquitin  
721 ligase-binding groove. The sidechains of A258 and V260 are embedded into binding pockets

722 too small to accommodate larger side chains<sup>32</sup>. They are in direct proximity of Siah residues  
723 T156 (pink) and M180 (cyan), identified as key binding residues in a series of pull-down  
724 assays<sup>32</sup>. The longer side-chains of A258T, A258S, A258V variants and the smaller V260G  
725 are likely to weaken or prevent the interaction with the ligase.

726 **(E)** Immunoblot showing the accumulation of mutated forms of AFF3 and AFF4 proteins  
727 compared to wild type (WT). Protein extracts of HEK293T cells independently expressing  
728 FLAG-tagged AFF3<sup>WT</sup>, AFF3<sup>A258S</sup>, AFF3<sup>V260G</sup>, AFF4<sup>WT</sup> and AFF3<sup>R258W</sup> proteins were  
729 immunoblotted with an anti-FLAG antibody (upper portion) and an anti-β-actin antibody for  
730 loading control (bottom portion). The positions of FLAG-AFF3, FLAG-AFF4 and β-actin  
731 proteins are indicated on the right; they are 133kD, 127kD and 42kD respectively. Signal  
732 intensity is measured and normalized on corresponding loading control.

733

734 **Figure 2: Photographs of KINSSHIP individuals with *AFF3 de novo* missense variants**

735 **(A)** Proband 2 at 2 years 6 months old;

736 **(B, I)** Proband 3 at 18 years old;

737 **(C)** Proband 4 at 9 months and **(D, J)** 21 years old;

738 **(E)** Proband 5 at 1 year 7 months and **(N-O)** 16 days old;

739 **(F, K-M)** Proband 6 at 9 years old;

740 **(G)** Proband 7 at 8 years old;

741 **(H, P-R)** Proband 8 at 7 years 9 months old;

742 **(S)** Proband 10 at 11 years old.

743 Note the synophrys and micrognathia, protruding ears, large nose with prominent nasal tip  
744 and prominent teeth in proband 3 **(B)**, 4 **(D)**, 6 **(F)** and 8 **(H)**, as well as their hypertrichosis of  
745 the limbs **(I, J, M, P)**. Together with probands 5 and 7, they exhibit thick hair, long eyelashes  
746 and a wide mouth **(E, G)**. Facial features coarsen with age as shown by pictures of proband 4  
747 at different ages **(C-D)**, explaining the more delicate features of younger probands **(A, E)**.

748 *AFF3 de novo* missense variant carriers also have hypoplastic talipes and abnormalities of  
749 toes **(I, J, M-S)**. Proband 6 also shows clinodactyly and soft tissue syndactyly of both hands  
750 **(K, L)**.

751

752 **Figure 3: X-rays of KINSSHIP individuals with *de novo* missense variants in *AFF3***

753 **(A-D)** Proband 3 at 18 years old;

754 **(E-I)** Proband 4 at 21 years old;

755 **(J-L)** Proband 5 at 10 months old;

756 **(M)** Proband 7 at 8 years old;  
757 **(N-P)** Proband 10 at 10 years old.  
758 **(A)** Severe scoliosis and fusion of C2-C3 vertebral bodies and L5-S1 vertebral cleft **(B)**  
759 Dorsal and radial bowing of the radius and "V-shaped" proximal carpal bones as seen in  
760 Madelung deformity, **(C)** metaphyseal widening and hypoplastic fibula and **(D)** hypoplastic  
761 talipes. **(E)** Static scoliosis, **(F)** Short ulna and radius and bilateral dislocation/subluxation of  
762 radial heads. Note erratic articulation of the styloid process of the ulna on the radius rather  
763 than on the carpal bones, **(G)** Congenital fusion of the bases of the second and third right  
764 metatarsals, **(H)** Hypoplastic bowing femora and **(I)** short tibias with enlarged metaphyses.  
765 **(J)** Right foot with 4<sup>th</sup> and 5<sup>th</sup> metatarsals synostosis **(K)** and left foot missing the lateral ray,  
766 **(L)** Extremely short rectangular fibula and bowed tibia. **(M)** Hypoplastic fibula. **(N)** Scoliosis  
767 and cervical ribs, **(O)** bowed radius and ulna, **(P)** bowed tibia, severely hypoplastic fibula and  
768 oligodactyly.

769

#### 770 **Figure 4: Neuroanatomical defects in *Aff3*<sup>-/-</sup> mice**

771 Merged double-stained sections in *Aff3*<sup>-/-</sup> mice (right of dashed lines) and their matched  
772 controls (WT: wild type, left of dashed lines) at the striatum **(A)** and at the hippocampus **(B)**  
773 levels with schematic representation of the affected areas **(C,D)**. Histograms showing the  
774 percentage of increase or decrease of parameters in measured areas as compared to the  
775 controls, for striatum **(E)** and hippocampus **(F)** sections. Red shading is proportional to the  
776 stringency of the significance threshold. Numbers indicate studied areas: 1=total brain area,  
777 2=lateral ventricles, 3=cingulate cortex (section 1) and retrosplenial cortex (section2),  
778 4=corpus callosum, 5=caudate putamen (section 1) and hippocampus (section 2), 6=anterior  
779 commissure (section 1) and amygdala (section 2), 7=piriform cortex, 8=motor cortex,  
780 9=somatosensory cortex, 10=mammilo-thalamic tract, 11=internal capsule, 12=optic tract,  
781 13=fimbria, 14=habenular, 15=hypothalamus, and 16=third ventricle. Results demonstrate an  
782 enlargement of lateral ventricles (**LV**; p=1.24E-04 on section 1, p=4.64E-02 on section 2) and  
783 a smaller genu of the corpus callosum (**gcc**; decreased corpus callosum size p=6.35E-02  
784 indicated by the black dash and double arrow, decreased bottom width of the corpus callosum  
785 p=3.02E-06 and decreased height of the corpus callosum p=4.96E-02). Other phenotypes of  
786 lesser stringency can be observed such as atrophy of the anterior commissure (**aca**; p=1.02E-  
787 02) and smaller hippocampus (p=4.02E-02).

788

#### 789 **Figure 5: Animal models**



790 **(A)** Schematic representation of the deletion generated in mice ES cells with the  
791 CRISPR/Cas9 system, which models the mutation observed in the deletion proband<sup>15,35</sup>.  
792 **(B)** Skeletal staining of E18.5 mouse embryos show mesomelic dysplasia with triangular tibia  
793 and hypoplastic fibula (see Figure 3 in reference<sup>35</sup>), as well as a hypoplastic pelvis in *Aff3<sup>del/del</sup>*  
794 mice, especially noticeable in the iliac wing (black arrows) and acetabulum (orange arrows),  
795 perturbations also observed in the deletion proband.  
796 **(C)** Delayed ossification of flat bones in the skull of *Aff3<sup>del/del</sup>* mice.  
797 **(D)** Lateral (top line) and dorsal (bottom line) views of the observed phenotypes of 4 dpf AB-  
798 WT zebrafish embryos injected with human AFF3 mRNA (hAFF3). hAFF3-injected  
799 zebrafish embryos exhibit severe developmental defects including a bent body axis and yolk  
800 sac edema (D3-6), as well as extreme malformations with absence of body axis, tail and fins  
801 and cyclopia (D7-8). Embryos with normal development are displayed for comparison (D1-  
802 2).  
803 **(E)** Proportions of normal and developmentally defective 4 dpf AB-WT zebrafish embryos  
804 upon injection of increasing doses of hAFF3 (left panel) and hAFF4 (right panel) mRNA.  
805 Dark and light colors indicate developmentally defective and normal animals, respectively.  
806 Control injections with Phenol Red show no significant (ns) differences with WT in both  
807 AFF3 and AFF4 experiments (Fisher exact test,  $p=0.09$  and  $p=0.12$  respectively). hAFF3  
808 mRNA injection significantly increases the number of zebrafish with developmental defects  
809 when compared to controls starting from 150ng (\*;  $p=0.03$ ) and reinforced at 300ng (\*\*\*)  
810  $p=3.2E-5$ ). AFF4 injections do not have a significant impact on zebrafish development  
811 compared to WT, even at the same dose (300ng,  $p=0.29$ ).

812

### 813 **Figure 6: *AFF2*, *AFF3* and *AFF4* targets**

814 **(A)** Venn diagram of the differentially expressed genes from independent RNAi of *AFF2*,  
815 *AFF3*, and *AFF4* (adapted from Luo et al<sup>47</sup>) showing that ALF transcription factors have  
816 different targets. The knocked-down gene color code is indicated on the right.

817 The expression modifications of common targets are presented in panels **B-E**. Common  
818 differentially expressed genes show adverse regulation between knockdown of *AFF3* and  
819 *AFF4* (**B**), *AFF2* and *AFF4* (**E**) and *AFF2/AFF3* and *AFF4* (**C**). Whereas RNAi of *AFF2* and  
820 *AFF3* similarly influence their 76 common targets (**D**), knockdowns of *AFF2* or *AFF3* have  
821 opposite effects to that of *AFF4* on their common targets [ $54/64=84\%$  (**E**) and  $119/125=95\%$   
822 (**B**) of common targets with opposite perturbation of their expression levels, respectively].

823

<b>Table 1. Predicted pathogenicity and allele frequencies of <i>AFF3</i> de novo variants</b>											
Gene	Individual	Chromosome coordinates (GRCh37/hg19)	Nucleotide change	Amino acid change	dbSNP (v152)	GnomAD allele frequency (v2.1.1)	Deleteriousness prediction (score)				
							CADD_PHRED (GRCh37-v1.4)	SIFT (v4.0.3)	PROVEAN (v1.1)	PolyPhen2 (v2.2.2)	Mutation Taster2 (09.01.19)
<i>AFF3</i> NM_001025108.1 NP_001020279.1	1	Chr2:100623270	c.772G>T	A258S	-	0	23.8	Damaging (0.000)	Neutral (-2.48)	Probably damaging (1.000)	Disease causing
	2										
	3	Chr2:100623270	c. 772G>A	A258T	rs1131692272	0	24.3	Damaging (0.000)	Deleterious (-3.30)	Probably damaging (1.000)	Disease causing
	4										
	5										
	6										
	7										
	8										
	9	Chr2:100623269	c.773C>T	A258V	-	0	24.2	Damaging (0.000)	Deleterious (-3.30)	Probably damaging (1.000)	Disease causing
	10	Chr2:100623263	c. 779T>G	V260G	-	0	24.4	Damaging (0.000)	Deleterious (-5.85)	Probably damaging (1.000)	Disease causing

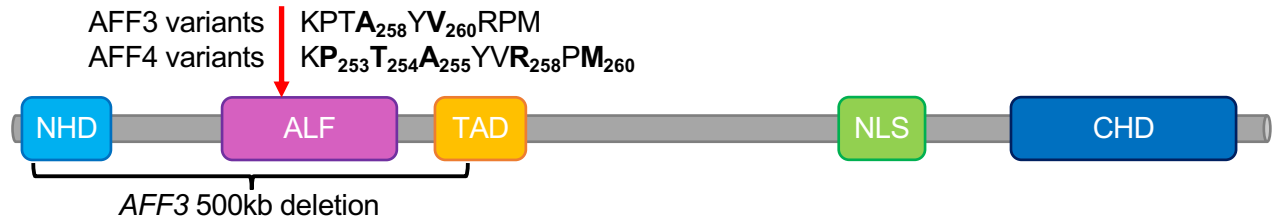
**Footnote:** SIFT cutoff=0.05, PROVEAN cutoff=-2.5, PolyPhen2 cutoff=0.5.

Table 2: <i>Aff3</i> mice models and their phenotypes							
Producer		IMPC <sup>33</sup>		Kraft et. al. <sup>35</sup>	This work		
Background		<i>C57BL/6N</i>		CD1	CD1	<i>C57BL/6N</i>	
Genotype		<i>Aff3</i> <sup>+/-</sup>	<i>Aff3</i> <sup>-/-</sup>	<i>Aff3</i> <sup>-/-</sup>	<i>Aff3</i> <sup>del/+</sup>	<i>Aff3</i> <sup>del/del</sup>	<i>Aff3</i> <sup>A233T</sup>
Phenotype	Craniofacial anomalies	-	+	NA	Variable features, from non-affected to homozygous-like phenotype	+	NA
	Vertebral malformations	+	+	NA		NA	
	Mesomelic dysplasia	-	-	-		+ *	
	Polydactyly	-	-	-		+	
	Kidney malfunction	-	+	NA		NA	
	Intestinal prolapse	-	-	NA		+	
	Neurological dysfunctions	-	+	NA		+	
	Neuroanatomical defects	NA	+	NA		NA	
	Reduced body size	-	-	NA		+	
	Lethality	-	-	NA	Low chimerism, no heterozygous offspring, suggesting lethality	Postnatal lethality	No heterozygous offspring, suggesting lethality

NA: Not available; IMPC significance threshold  $p \leq 10^{-04}$ , \*Kraft et. al<sup>35</sup>

5

**A**



**B**

← degron →

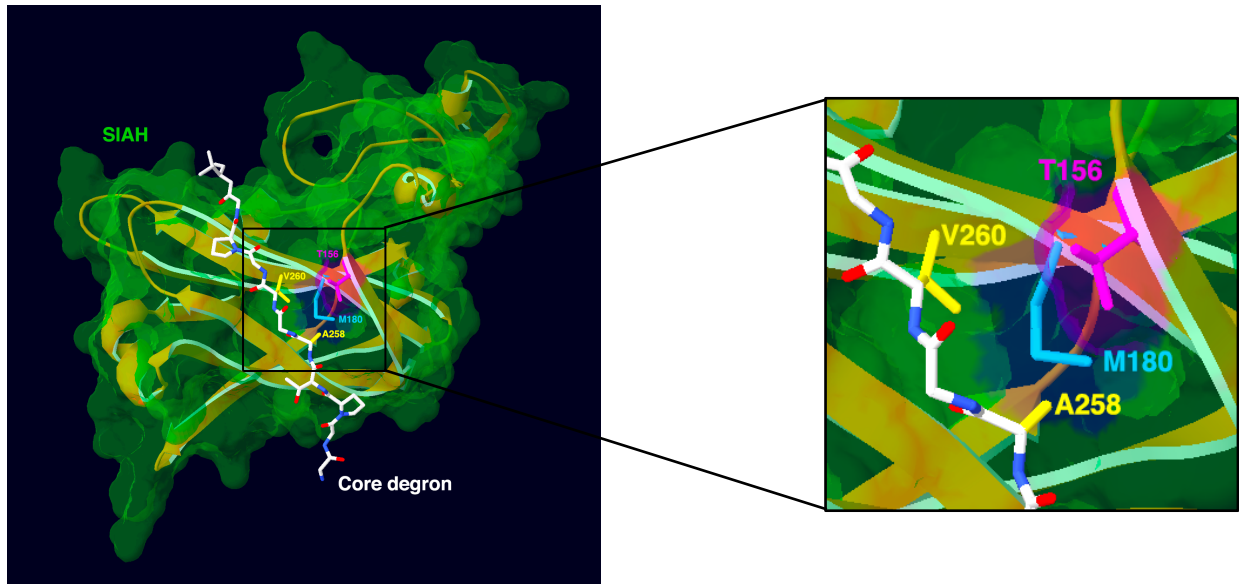
AFF1	272	QTFPPPSLP	SKSVAMQQ	KPTAYVRPM	DGQDQAP	SESP	ELKLP	ED	316
AFF2	268	QNF-PPGLYCKT	SMGQQ	KPTAYVRPM	DGQDQAP	DISPT	LKPSI	EF	311
AFF3	239	QNF-PPSLASKPSLVQQ	KPTAYVRPM	DGQDQAP	DESP	KLKSS	SET	282	
AFF4	236	QSF-PPSLMSKNSMLQ	KPTAYVRPM	DGQ	ESMEPK	- - -	L - -	SSEH	274

**C**

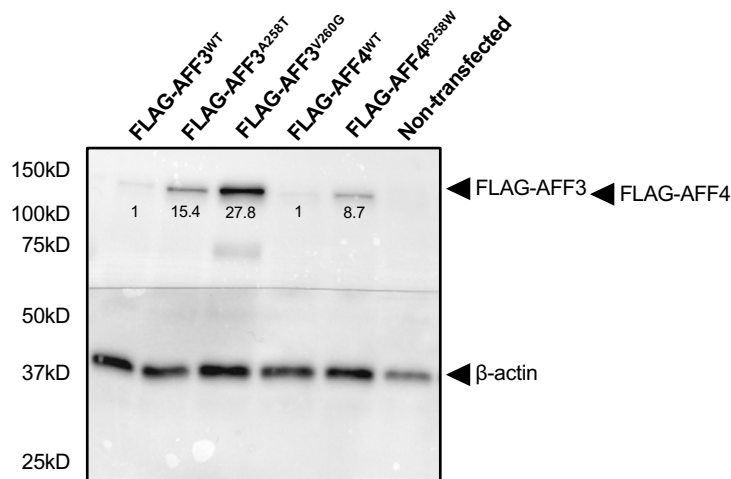
x P x A x V x P x

Human	239	QNFPPSL	- - ASKPSLVQQ	KPTAYVRPM	DGQDQAP	DESP	- KLKSS	SET	282
Mouse	214	QNFPPSL	- - ASKPSLVQQ	KPTAYVRPM	DGQDQAP	DESP	- KLKS	STET	257
Cat	220	QNFPPSL	- - ASKPSLVQQ	KPTAYVRPM	DGQDQAP	DESP	- KLKS	STET	263
Elephant	224	QNFPPSL	- - ASKPSLVQQ	KPTAYVRPM	DGQDQAP	DESP	- KLKS	STET	267
Chinese Turtle	171	QNFPPSL	- - ASKPNIVQQ	KPTAYVRPM	DGQDQAP	DESP	- KLKLL	SES	214
Anole Lizard	247	QNFPPS	- - - - KPSIVQQ	KPTAYVRPM	DGQDQAP	DESP	- RLKVP	PAET	287
Lamprey	245	QAFPSL	LPVSSKQSS	LQQKPTAYVRPM	DGQDQ	QLSSDC	SEL	PSSSGP	291

**D**



**E**



*Because rapid and automated nature of preprint posting are incompatible with verification of informed consents, Biorxiv prohibits us to show these panels A-H.*

*Facial phenotypes are detailed in text and legends.*





